Biomass and Bioenergy 193 (2025) 107563

Contents lists available at ScienceDirect

Biomass and Bioenergy

journal homepage: www.elsevier.com/locate/biombioe

Ash partitioning in combustion of pelletized residual agricultural biomass

Javier Royo *, Paula Canalís, David Quintana

University of Zaragoza, C/ María de Luna 3, E-50018 Zaragoza, Spain

ARTICLE INFO

Keywords:
Biomass combustion
Agropellet
Ash partitioning
Fixed bed reactor
Bottom ash sintering
Ash deposition

ABSTRACT

The use of residual agricultural biomass in the domestic sector has faced limitations for years due to the problems caused by the characteristics of its ash (quantity and composition). Quantifying and characterizing the fractions into which ash is divided during combustion process can help overcome this barrier. Based on ash samples from tests carried out in a laboratory fixed-grate reactor, a methodology for the analysis of ash partitioning during combustion has been presented and applied to four agropellets (one woody and three blended with herbaceous component –mixed agropellets-), both at the ash level and of the main chemical elements that constitute it. Ash has been separated in five fractions, analyzing the results considering the fuel composition and the operating conditions. In addition to detecting important differences in the partitioning among tested fuels, especially between mixed agropellets and the woody one, it should be noted that the analysis of elemental partitioning has shown that the order in the retained percentage of each element in the bottom ash fraction is Si > Ca + Mg > P > K + Na for all agropellets. An increment in the excess air has been corroborated to improve the behavior of the tested mixed agropellets both in sintering and in deposition. In case of the woody pellet, as its much lower sintering status supposes a dominance of fractions related with entrainment, it is preferable working with low excess air. The presented methodology allows estimating the importance and composition of each fraction, which affect the operation and condition the boiler design and is of great importance to achieve larger use of this kind of biomass.

1. Introduction

The growth of the energetic utilization of residual agricultural biomass, mainly herbaceous crop residues and pruning residues of permanent woody crops, is essential if the objectives set for 2030 in terms of reduction in greenhouse gases emissions and share of renewable energy consumption are to be achieved [1]. These are very abundant resources all across Europe [2], which do not compete with other land uses [3], and whose use as an energy source can be compatible with other applications [4].

However, in order for its great potential to be truly utilized, it is necessary to overcome certain singularities of these fuels essentially related to the characteristics of their ash (quantity and composition), especially in the herbaceous agricultural biomass.

During combustion, ash undergoes physical and chemical transformations which cause its partitioning. Part of the components of the ash gives rise to a solid fraction which accumulates in the grate (bottom ash). Under certain combustion conditions and when the fuel ash fusion temperatures are sufficiently low, the bottom ash can sinter and cause serious equipment problems, affecting the conversion in the bed, restricting the effectivity of the grate and negatively influencing proper control of gaseous emissions ([5–9]). The main phenomenon causing sintering consists in the formation of low-melting alkali metal silicates, mainly K. The low eutectic temperatures of K_2O-SiO_2 system, which can be as low as 600 °C [10], are a critical factor in this phenomenon. Bottom ash sintering through this mechanism is especially remarkable in herbaceous fuels compared to woody biomass, since its ash content is generally higher, as well as its concentration of Si and K [11]. Phosphorus shares certain behaviors with Si, playing an important role in sintering in biomasses with a high content of this element. Since P is preferential over Si in the initial interaction with alkali metals [12], K (Na)- Phosphates can be formed which, as K (Na)- Silicates, also have a low melting temperature.

The part of the ash which is not retained in the bed (fly ash) can leave it through two different mechanisms: vaporization and entrainment of solid particles (coarse fly ash). Regarding Si, compounds containing it can leave the bed only through entrainment,[1] since Si is considered a

* Corresponding author. author.
E-mail address: fjroyo@unizar.es (J. Royo).

[1] Vaporization of Si might occur at high temperatures and in reduced atmospheres [10], but Si-gaseous species are considered as highly reactive, forming solid compounds which can stay in the bed or be entrained.

https://doi.org/10.1016/j.biombioe.2024.107563
Received 20 September 2024; Received in revised form 3 December 2024; Accepted 15 December 2024
Available online 2 January 2025

Abbreviations

%m/m	mass percentage
Chim/Ind	Ash fraction that come out of chimney and the indeterminate ones (%)
d.b	dry basis
Dep:	Ash fraction deposited by condensation and by inertial impact (%)
DepC	Ash fraction deposited by condensation (%)
DepI	Ash fraction deposited by inertial impact (%)
DR	Deposition Rate ($g{\cdot}m^{-2}{\cdot}h^{-1}$)
EDS	Energy Dispersive X-ray Spectrometry
HHV	High heating value ($MJ{\cdot}kg^{-1}$)
Int. 1.5	Value of the corresponding fraction obtained from the trend line for a λ of 1.5 (%)
LHV	Low heating value ($MJ{\cdot}kg^{-1}$)
PV	Vineyard pruning agropellet
PVB	Vineyard pruning and Barley straw mixed agropellets
PVC	Vineyard pruning and Corn stover mixed agropellets
PVCB	Vineyard pruning, Corn stover and Barley straw mixed agropellets
S1	Bottom ash fraction not sintered (%)
S2	Bottom ash fraction with low sintering status (%)
S2/3	Fraction S2 plus fraction S3 (%)
S3	Bottom ash fraction with high sintering status (%)
SEM	Scanning Electron Microscopy
Ta	Inlet air temperature (°C)
TC3m	Mean flame temperature (°C)
TCi	Temperature registered by the thermocouple located in position i
w.b	wet basis
V_{PA}	Air velocity in the grate ($m{\cdot}s^{-1}$)
λ	Excess air ratio

refractory element [10]. Conversely, K + Na can react with Cl, S and H to form volatile compounds: mainly K (Na)- Sulfates, K (Na)- Chlorides and K (Na)- Hydroxides (which can subsequently give rise to K (Na)- Carbonates). In respect of P, its importance on partitioning is clear, since the fact that K (Na)- Phosphates are even more stable than the mentioned K (Na)- Sulfates, K (Na)- Chlorides and K (Na)- Carbonates [13] can drastically change the volatilization processes and increase the SO_2/SO_3 and HCl emissions (by decreasing the reactions between S, Cl and O with alkali metals). P can also form compounds which volatilize with high enough combustion temperatures [10], especially when the P/Si molar ratio is high ([13–15]), although to a lesser extent than K + Na. Ca and Mg are considered very refractory [10], although some authors point out that they can vaporize to certain degree (see for example [16] or [17]), but they do not clarify the compounds involved in this vaporization. Another characteristic of alkaline earth metals is that at high temperatures they can form oxides, CaO and MgO, through several possible pathways and will probably be released as small micrometer-sized particles [10]. One of these pathways is the decomposition of carbonates such as calcite ($CaCO_3$), reaching a complete conversion to oxide between 650 and 900 °C ([18,19]), but there are other ways such as through anhydrite ($CaSO_4$) desulfation at 800–1300 °C [20]. In other words, it can be seen that whether Ca/Mg-containing compounds vaporize or form micrometric particles that are easily entrained, the release of Ca and Mg from the bed could increase with combustion temperature.

Following complex mechanisms ([21,22]), part of the volatilized compounds can directly condense or after forming aerosols be deposited by thermophoresis and/or turbulent diffusion ([22–24]) on the heat exchange surfaces of the equipment, in the form of small crystals (e.g., potassium chloride -KCl-, potassium sulfate -K_2SO_4- and potassium carbonates -K_2CO_3 and $KHCO_3$). Other part can even condense into coarse fly ash ([22,23]). On the other hand, in some conditions coarse fly ash particles can be deposited on heat exchange surfaces by inertial impact. All these deposits are responsible, besides the worsening in heat transfer, for corrosion and erosion in those surfaces, reducing performance and lifetime of the equipment ([5–9]).

Finally, part of the fly ash, instead of leading to deposits formation, comes out of the chimney along with the combustion gases in the form of aerosols. Thus, some fractions of the finer particles (mostly those of size below 10 μm or even 2.5 μm), can end up being emitted to the atmosphere, causing respiratory diseases ([25,26]). Those particles could include crystalline silica entrained from the bed (particularly in the form of quartz and cristobalite, that are carcinogens [27]). It should be also considered the compounds that remain in gaseous state and that are also emitted by the chimney, such as sulfur dioxide -SO_2- or hydrogen chloride -HCl-which, although they account for small concentrations, are environmental pollutants ([28,29]).

Several studies on biomass ash partitioning during combustion can be found in the literature, in which the main aim is closing the ash mass balance (e.g. Refs. [30–34]). However, they usually focus on bottom and fly ash, but not analyze in depth the part of the latter that is deposited on heat exchange surfaces.

This article presents a new methodology for analyzing biomass partitioning that includes five fractions, two of them related to deposition (based on through which of the two mechanisms the ash leaves the bed), which is one of the phenomena that most affect the boilers performance.

In addition to this ash mass balance, from the elemental composition of the deposits and bottom ash fractions, mass balance will be also presented at the elemental level, which will allow knowing how the most relevant chemical elements of the fuel ash are distributed between the different fractions, allowing a more complete analysis of the complex partitioning processes.

The variable quantity of each of these fractions along with their composition affect the operation and determines up to a point the design of various boiler systems. Advancing in the characterization of the fractions can therefore be of vital importance in order to achieve a larger use of the agricultural residual biomass.

As an example of the application of this methodology, the ash partitioning of four pellets made of residual agricultural biomass (agropellets) has been analyzed, studying the influence of the operating conditions such as excess air ratio (λ) and inlet air temperature (Ta). These two parameters vary the combustion temperature and the air velocity in the bed, directly influencing the different fractions. This study starts from an extensive test campaign carry out in a laboratory fixed-grate reactor ([35–37]) and its subsequent results analysis, in which it was determined the influence of the fuel composition and the operating conditions on the combustion parameters, the sintering degree and the deposition rate [35]. The mechanisms of deposition [36] and sintering [37] were also analyzed in depth. This application example aims to show how the methodology is useful to advance the understanding of the behavior of biomass fuels.

2. Material and methods

2.1. Fuels

Three agricultural residual biomasses (two herbaceous and one woody) were selected due to their wide availability in both Europe and the rest of the world [36]: vineyard pruning residues, barley straw and

corn stover. Given these raw materials, four different agropellets (agricultural residual pellets) were produced.

- Woody agropellet: 100 % Vineyard pruning pellet (PV)[2]
- Mixed agropellets (Vineyard pruning blended with a herbaceous component):
  - o 70 % Vineyard pruning + 30 % Barley straw (PVB)
  - o 70 % Vineyard pruning + 30 % Corn stover (PVC)
  - o 60 % Vineyard pruning + 20 % Corn stover + 20 % Barley straw (PVCB)

The three mixed agropellets were designed to meet the requirements of the ISO 17225–6:2014 standard for non woody pellets, both A class (PVB) and B class (PVC and PVCB), the limiting parameters being the ash and Cl contents. The main thermochemical properties of the four fuels used are reproduced from Ref. [35] and presented in Tables 1 and 2[3].

2.2. Reactor

In order to perform the combustion tests, an experimental fixed-grate reactor was used (see Fig. 1). In this reactor, inlet air is injected through the grate from the bottom by means of a fan equipped with a variable-frequency drive which allows regulating the airflow. Since experiments require inlet air temperature (Ta) to remain under control, the reactor is equipped with a refrigerator and an electrical resistor either to cool the air or heat it as needed. It allowed two different types of tests to be undertaken: without air preheating (Ta = 25 °C) and with air preheating (Ta = 80 °C). The reactor is fitted with fifteen type N thermocouples to monitor the temperature both at the bed and the freeboard. For identification purposes, they are numbered from TC1, the closest to the grate, to TC15, located in the upper part of the reactor. Based on the recorded temperatures, it is possible to estimate the mean flame temperature (TC3m, °C) as the average value of the temperature registered by TC3 in the interval between TC2 and TC1 reaching 500 °C. TC3m is considered in the results analysis as a representative parameter of the combustion temperature just above the bed for the present experimental tests.

In addition, the facility is completed by installing a deposition probe, with a removable sampling ring in the chimney of the reactor (see further description in Ref. [38]). This is a common device used to simulate fly ash deposition in furnace pipes and heat exchangers [39].

For more details about characteristics, operation and controlling of the reactor see Ref. [35].

Table 1
Fuel properties.

		PV	PVB	PVC	PVCB
Bulk density (kg·m^{-3})[a]		599	562	556	546
Proximate analysis (% m/m d.b)	Volatile matter[b]	76.5	72.4	72.1	72.3
	Fixed carbon[c]	20.4	21.7	18.6	21.2
	Ash[d]	3.1	5.9	9.3	6.5
Total Moisture (% m/m w.b.)[e]		9.0	9.1	9.2	9.0
Ultimate analysis (% m/m d.b.)	Carbon[f]	48.90	46.36	46.01	46.36
	Hydrogen[f]	5.80	5.77	5.64	5.55
	Nitrogen[f]	.55	.56	.55	.60
	Sulfur[g]	.090	.055	.050	.094
	Chlorine[g]	.030	.047	.080	.090
	Oxygen[c]	41.60	41.29	38.33	40.58
HHV (d.b. At p = constant) (MJ·kg^{-1})[h]		19.11	18.54	18.06	18.36
LHV (w.b. At p = constant) (MJ·kg^{-1})[h]		16.01	15.48	15.06	15.40

[a] EN 15103:2009.
[b] EN-ISO 18123:2016.
[c] Calculated.
[d] EN-ISO 18122:2016.
[e] EN-ISO 18134:2016.
[f] EN-ISO 16948:2015.
[g] EN-ISO 16994:2015.
[h] EN-ISO 14918:2011.

2.3. Ash analysis

In the test, once combustion was completed and the reactor cooled down, bottom ash was collected from the grate for weighing and classification, which allowed determining the tendency to sinter of each fuel ([5,14,32,40–42]). The following categories, based on a revised classification of sintering status defined in previous works ([14,42]), were used: S1, ash which passes through a 3.15 mm sieve and is considered not to be sintered; S2, ash which does not pass through a 3.15 mm sieve, but is easily disaggregated by hand pressure, indicative of low sintering status; S3, ash which does not pass the 3.15 mm sieve, and is difficult to disaggregate by hand pressure, which is indicative of high sintering status. To avoid the subjectivity involved in separating these last two fractions by hand pressure, both have been grouped in a single category (S2/3) as it has been done in other studies that used the same methodology to classify the bottom ash (e.g. Ref. [32]). In this work and in previous publications ([35–37]) the sintering degree of a fuel was defined as the percentage of this last fraction (S2/3) with respect to the total ash introduced with the fuel in each test. The higher this percentage, the more problematic the fuel is considered.

On the other hand, the deposition rate (DR, g·m^{-2}·h^{-1}) calculated based on the difference in weight between the clean sample ring (before introducing into the chimney) and the dirty sample (with the deposit sample collected during the test) allowed estimating the tendency to deposition of each studied fuel ([43–48]).

For all the tests, once deposits had been weighed and DR calculated, a sample was taken from the front face of the removable sampling rings, that is, from the side facing and perpendicular to the flow of combustion gases. Samples of S1 and S2/3 bottom ash fractions were also collected and crushed in a mortar to obtain a homogeneous mixture with an adequate particle size to be analyzed. Each one of these samples were glued onto metal plates with carbon tape and then coated with carbon before being analyzed by SEM-EDS method. This technique has been used to determine the elemental composition of ash by a large number of researchers (e.g. Refs. [32–34,49–51]), and, in this case, it is the most convenient option considering the high number of samples treated and the low amount of deposits available. The equipment used was a Carl Zeiss Merlin electronic field emission microscope equipped with Gemini Column, with acceleration voltages between .02 and 30 kV, fitted with an EDS for the analysis of the energy of scattered X-rays, X-MAS detector by Oxford Instruments, with a window of 20 mm^2 and energy resolution between 123 eV and 5.9 keV of Mn Kα. For each sample, three 1- mm^2 representative zones were selected using the angle selective backscattered electron detector (AsB). Average elemental composition was obtained through EDS, using a voltage of 15 kV to obtain information on the elements present in the sample. Major participating elements in the most important ash transformation processes – namely Na, Mg, Al, Si, P, S, Cl, K, Ca and Fe – were included in the analysis. INCA software was used to process the results.

2.4. Statistical analysis

In order to determine the goodness of the linear correlations shown in section 4, a statistical analysis through the estimation of Pearson's correlation coefficient (r) and its corresponding p-value (p) was

[2] Vineyard pruning raw material used to produce this agropellet were not the same as those used for mixed agropellets.
[3] The samples to be analyzed were collected following the guidelines set out by the ISO 14778:2013 standard.

Table 2
Fuel ash properties.

		PV	PVB	PVC	PVCB
Chemical ash composition (% m/m d.b.)[a]	Al_2O_3	.91	2.72	2.19	2.30
	CaO	42.39	45.77	48.17	40.54
	Fe_2O_3	.71	2.22	1.98	1.27
	K_2O	30.09	14.88	15.79	19.43
	MgO	10.45	8.64	7.64	11.01
	Na_2O	.62	.41	.39	.38
	P_2O_5	7.35	4.45	4.00	4.36
	SO_3	3.95	2.32	3.24	4.39
	SiO_2	2.65	17.70	15.31	15.22
	TiO_2	.07	.17	.18	.16
	Cl	.12	.21	.57	.54
Ash melting temperatures oxidant conditions (°C)[b]	Initial deformation temperature	1240	1130	1310	1330
	Hemisphere temperature	>1500	1310	1460	1460
	Flow temperature	>1500	1370	1480	1470

[a] EN-ISO 16967:2015.
[b] C EN/TS 15370–1:2006.

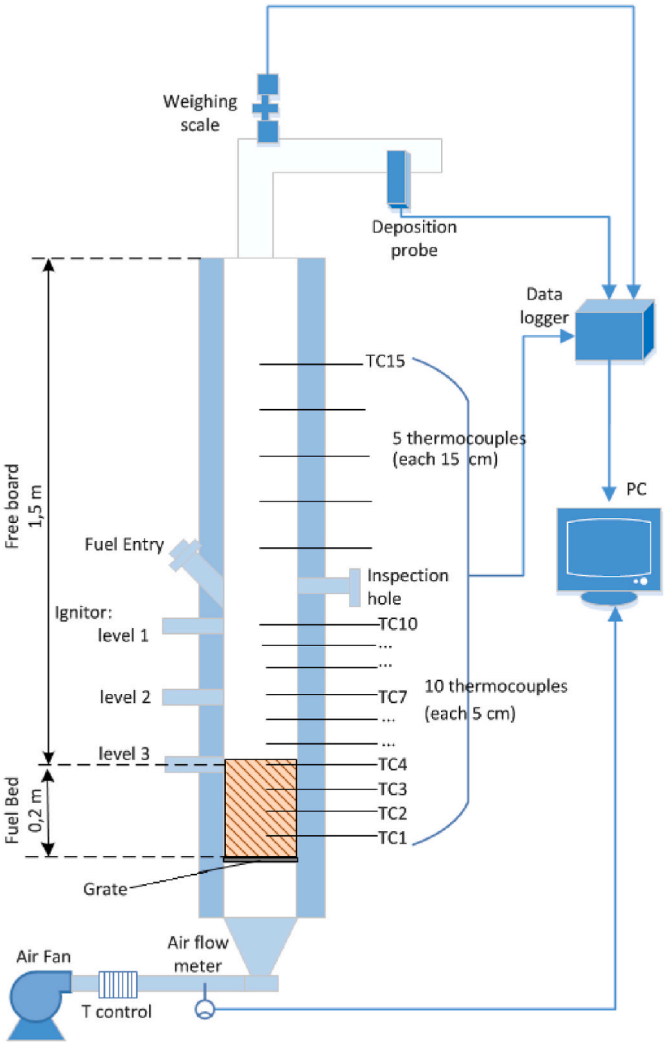

Fig. 1. Scheme of the experimental test facility [35].

undertaken. A correlation is considered statistically significant when $p < .05$.

3. Test features and summary of previous results

A total of 68 combustion tests were carried out with the four fuels following the same protocol. Detailed information about this experimental protocol can be found in Ref. [35]. Table 3 summarizes the main features and results of the experiments performed. Tests both with and without preheating were undertaken for every fuel by varying Ta. In this work, preheated tests (named as "ph" experiments) are used to confirm the trends in the influence of TC3m and air velocity (V_{PA}) on ash partitioning (section 5.2). λ value used was greater than 1 (over-stoichiometric conditions) in all tests, in order to reproduce the combustion conditions found in small domestic equipment (without secondary air).

In the same table, mean value (and range) of the results obtained in the tests in relation to the S2/3 fraction and DR are presented. Mean values (and range) of elemental composition obtained by SEM-EDS for each of the four fuels for S1 and S2/3 bottom ash fractions, as well as for the fly ash deposits are also shown. Due to their chemical similarity and the almost identical role that they play in the reactions that take place in ash transformation processes, the concentrations of K and Na [10], as well as Ca and Mg [52], have been aggregated. Greater detail of the results obtained in the tests and their subsequent analysis are available at [35–37]. Also, the presence of certain crystalline species detected by P-XRD method and the analysis of their transformation can be found in Ref. [36] for deposits and in Ref. [37] for bottom ash.

4. Ash partitioning: methodology and processed results

The analysis of the results from the test campaign conducted with the reactor allowed in the abovementioned publications to confirm the existence of correlation between the values of the sintering degree and the deposition rate, as well as the influence of the operation conditions on them.

To deepen this analysis and better understand the ash partitioning behavior both in terms of the influence of the fuel composition and the operation conditions, a mass balance of the fuel ash (ash partitioning) and balances of each one of its most relevant chemical elements (elemental partitioning) are performed. To do this, in this work ash is

Table 3
Outline of test features and main test results, mean value and (range).

			Without preheating tests (Ta = 25 °C)				Preheated tests (Ta = 80 °C)			
			PV	PVB	PVC	PVCB	PV	PVB	PVC	PVCB
Number of tests performed			10	10	10	12	8	6	6	6
Fed fuel (kg)[a]			4.03	3.78	3.74	3.67	4.03	3.78	3.74	3.67
λ			1.52 (1.15–2.04)	1.61 (1.24–2.30)	1.67 (1.18–2.29)	1.59 (1.23–2.07)	1.46 (1.27–1.65)	1.59 (1.21–2.14)	1.35 (1.26–1.54)	1.41 (1.28–1.51)
Mean flame temperature (TC3m, °C)			1013 (894-1109)	963 (783-1079)	958 (778-1074)	952 (808-1056)	925 (846-1038)	1004 (913-1084)	1024 (984-1058)	1029 (1013-1052)
Air Velocity in the grate (V_{PA}, m·s^{-1})			8.01 (6.95–9.06)	8.11 (7.17–9.08)	8.44 (7.93–9.02)	8.00 (7.13–8.53)	10.97 (9.86–11.86)	11.20 (10.38–12.20)	11.60 (10.65–12.28)	10.97 (10.45–11.68)
S1 fraction (%)[b]			23.7 (17.0–29.4)	22.9 (11.9–50.9)	16.2 (8.4–26.8)	19.4 (9.5–33.2)	12.4 (9.5–16.5)	13.9 (9.6–18.2)	7.6 (6.6–8.1)	10.0 (8.6–12.5)
S2/3 fraction (%)[b]			1.6 (0.3–3.1)	51.8 (26.7–62.2)	33.8 (23.5–40.7)	40.1 (26.4–49.8)	0.6 (0.1–1.1)	58.5 (54.5–62.5)	40.2 (38.7–41.3)	45.9 (41.7–48.9)
Deposition rate (g·m^{-2}·h^{-1})			16.6 (11.0–21.3)	20.9 (10.5–29.9)	19.4 (14.2–25.0)	19.2 (13.5–23.8)	15.1 (10.4–23.6)	24.4 (18.7–28.1)	27.7 (25.6–31.7)	26.4 (24–31.1)
Elemental composition obtained by SEM-EDS	**S1 fraction (%m/m)**[c]	**Si**	2.41 (1.79–3.62)	11.23 (8.66–13.52)	12.28 (8.39–18.08)	13.52 (10.34–17.15)	2.86 (1.51–4.33)	12.59 (11.47–13.45)	13.74 (11.43–17.51)	14.16 (11.59–18.44)
		K + Na	28.63 (17.17–35.40)	24.53 (21.60–29.97)	12.45 (7.99–16.15)	19.77 (14.22–22.78)	31.47 (24.53–34.67)	22.69 (20.84–26.01)	13.7 (11.26–15.47)	18.3 (15.98–22.62)
		Ca + Mg	60.34 (54.22–70.86)	55.52 (49.68–61.08)	68.44 (62.69–74.14)	58.56 (53.49–64.61)	57.54 (53.44–64.66)	56.66 (52.57–58.44)	65.98 (62.32–71.52)	60.60 (53.97–65.64)
		P	5.52 (4.95–6.21)	2.65 (2.32–2.83)	2.06 (1.11–2.59)	2.64 (1.87–3.03)	5.00 (4.13–4.43)	2.51 (2.29–2.75)	2.15 (1.83–2.50)	2.39 (2.02–2.87)
	S2/3 fraction (%m/m)[c]	**Si**	7.43 (3.47–18.51)	18.60 (13.27–23.93)	20.71 (15.14–24.83)	19.90 (14.43–24.31)	11.98 (2.72–24.02)	19.58 (17.38–21.47)	23.38 (21.98–26.06)	22.18 (20.03–24.76)
		K + Na	4.80 (1.06–11.12)	15.37 (9.58–18.19)	7.88 (6.20–9.86)	14.22 (10.89–19.06)	13.29 (6.77–20.50)	14.85 (12.44–18.27)	8.09 (6.72–9.54)	12.04 (10.47–13.65)
		Ca + Mg	78.53 (61.95–85.39)	59.41 (52.14–73.93)	66.41 (58.81–76.64)	59.27 (52.93–66.70)	66.87 (53.69–75.47)	59.6 (56.14–64.56)	63.72 (59.94–66.36)	59.99 (56.85–63.20)
		P	5.82 (2.97–7.56)	1.78 (1.13–2.14)	1.55 (1.07–2.06)	1.99 (1.68–2.35)	3.64 (1.39–6.24)	1.83 (1.59–2.11)	1.51 (1.16–1.76)	2.05 (1.91–2.15)
	Fly ash deposits (% m/m)[c]	**Si**	0.64 (0.40–0.86)	1.21 (0.57–1.81)	3.12 (1.39–4.54)	3.55 (2.26–5.31)	0.74 (0.59–0.91)	1.35 (0.50–2.27)	3.38 (2.10–3.97)	3.78 (1.87–5.08)
		K + Na	50.32 (40.62–58.60)	58.27 (53.46–62.45)	40.34 (28.61–49.88)	44.64 (33.07–53.51)	41.28 (34.70–47.81)	57.05 (53.61–60.71)	37.87 (33.95–46.54)	42.56 (37.37–52.46)
		Ca + Mg	32.46 (24.43–43.93)	7.66 (3.73–9.90)	27.06 (13.06–43.1)	24.51 (14.60–40.65)	40.86 (32.17–49.39)	8.65 (2.94–13.46)	32.71 (20.56–38.11)	29.12 (15.74–35.48)
		P	3.50 (2.40–3.30)	0.51 (0.25–0.69)	1.36 (0.74–2.41)	1.61 (0.88–2.71)	4.32 (3.12–5.14)	0.70 (0.29–1.11)	1.73 (1.22–2.30)	2.11 (1.28–2.66)

[a] Following ISO 14778:2013 standard
[b] % with regard to total mass of ash introduced with the fuel.
[c] Mean values (range) of the elemental composition(SEM-EDS) expressed as a percentage of the total mass of measured elements (Na, Mg, Al, Si, P, S, Cl, K Ca and Fe) (% m/m: mass percentage).

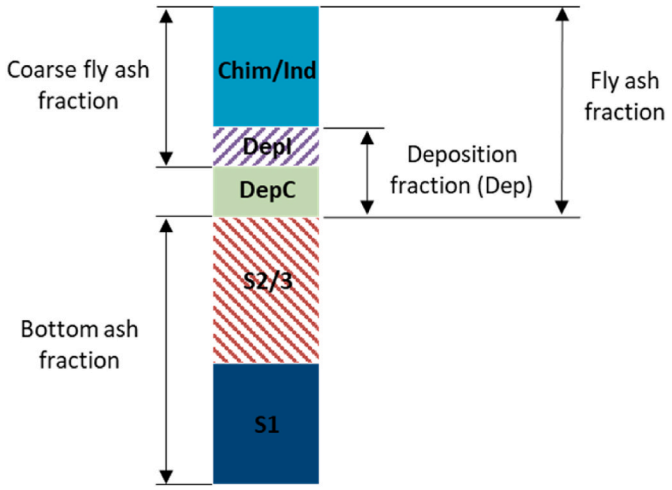

Fig. 2. Ash fractions distribution.

classified in five different fractions. Two of them (S1 and S2/3) corresponding to bottom ash with different sintering status. Two other fractions corresponding to deposits, separated by the mechanisms in which the ash leaves the bed: on the one hand, the deposition by condensation (DepC), associated with the ash that leaves the bed by vaporization and which includes the deposition by thermophoresis and turbulent diffusion; on the other hand, the deposition by inertial impact (DepI), associated with the ash that leaves the bed by entrainment. Lastly, a remaining fraction is defined, including the part of fly ash that come out of the chimney and the indeterminate matter (Chim/Ind). This last fraction could be considered to be mostly related to particle entrainment, although, along with the measurement uncertainties, it may also include some scarce vaporized species, mainly containing alkali metals compounds in the form of aerosols.

In certain points throughout the analysis, it is interesting to group some of these fractions (see Fig. 2).

- Bottom-ash-related fractions, resulting in bottom ash fraction (S1 + S2/3)
- Fly-ash-related fractions, resulting in fly ash fraction (DepC + DepI + Chim/Ind)
- Coarse-fly-ash-related fractions, resulting in coarse fly ash fraction (DepI + Chim/Ind, although the latter is included under the particularities explained above)
- Deposition-related fractions, resulting in deposition fraction (Dep = DepC + DepI)

4.1. Ash mass balance (ash partitioning)

The amount of ash belonging to fractions S1 and S2/3 was measured by weighing in the tests carried out. In order to know the amount of DepI and DepC, it is necessary to previously obtain the total amount of Dep. It is estimated by the deposition rates measured in the tests (DR), but additionally making two assumptions. In first place, the value of DR is considered constant over the entire heat exchange surfaces and equal to that obtained in the reactor tests. Secondly, a value of heat exchange surface per unit of heat transfer ratio of .09 $m^2\ kW^{-1}$ is used. This is an intermediate and representative value obtained by considering a typical overall heat transfer coefficient between gases and liquid water from 20 to 300 $W\ m^{-2}\ K^{-1}$ [53] and a logarithmic mean temperature difference from 300 to 400 K. To assess the influence that these assumptions have on the results obtained, a sensitivity analysis has been carried out, varying the value of the heat exchange surface per unit of heat transfer ratio between .06 and .12 $m^2\ kW^{-1}$. Some results of this analysis are shown in Appendix A, where it can be verified that the variation of this parameter does not have a determinant effect on the values of the fly-ash-related fractions, which maintain their order of magnitude and their relative weight. Their behavioral trends and the relative differences between fuels are also unaffected.

In order to determine the amount of ash corresponding to the DepI fraction, an extended methodology with respect to that proposed in Ref. [36] for dividing the DR into condensation and inertial impact is used. Thus, it is assumed that all Si present in the sampling ring have been deposited by inertial impact and that the ratio between Si and the main elements (Si/(K + Na + Ca + Mg + P)) in the DepI fraction is equal to that in S1,[4] since the latter fraction, due to its low sintering status, is the most similar to the ash entrained. Therefore, here it is taken into account that compounds containing other relevant elements apart from K and Na can also volatilize (and subsequently condense) or have greater ease of entrainment than Si. The importance of this additional condition will be discussed in depth in section 5. The DepC fraction is obtained as the difference between Dep and DepI. The Chim/Ind fraction is obtained by the difference between the other four fractions and the total mass of ash determined in the fuel analysis (Table 1).

Taking all this into consideration, Table 4 presents the mean values of the percentages of each fraction (with respect to the ash fed with the fuel) and their range, calculated following the explained methodology (only tests without preheating).

Apart from mean values which can be useful up to a certain extent, it is of special interest to analyze λ influence on partitioning. Fig. 3 shows the ash distribution against λ for each test without preheating of the four fuels. Appendix B presents the corresponding slope and intercept of the regression lines, as well as the Pearson's coefficient and p-value of the correlations between each fraction and λ, in order to determine whether these correlations are considered statistically significant and their relevance.

Also, the influence of air preheating on ash partitioning should be examined. Fig. 4 shows the mean values of tests with preheating, but also the values of tests without preheating. To avoid distortions due to very different λ values, only the non-preheated tests with a similar λ range to tests with preheating are used for fair comparison between both types of tests.

4.2. Elemental mass balance (elemental partitioning)

Approaching the phenomena that take place in ash partitioning from a complementary perspective, additional mass balances can be conducted at the level of the main chemical elements that make up the ash (Si, Ca + Mg, K + Na and P). As in the case of the ash partitioning, it is also possible to analyze the elemental partitioning, i.e., to determine what percentage of each element with respect to its total is found in each of the defined fractions.

For this purpose, an extra simplification to those made in 4.1 is needed: it is assumed that for each unit mass of ash there is approximately .5 units of Si + Ca + Mg + K + Na + Al + Fe, as justified in detail in Ref. [36].

The amount of any chemical element belonging to each S1, S2/3 and Dep fraction is estimated with the total mass amount of each fraction (subsection 4.1) and its composition (from SEM-EDS analysis, Table 3).

To get to know the composition of DepI and DepC fractions, since Si can only leave the bed by entrainment phenomenon, all deposited Si is accepted to belong to the DepI fraction. To determine the amount of the other elements present in DepI, the methodology presented in 4.1 is used, but expanding it to consider that the proportions Si/(K + Na), Si/(Ca + Mg) and Si/P in the DepI fraction are the same as in the S1

[4] In Ref. [36], in order to determine the percentage of DR that was caused by inertial impact, only the Si/(K + Na) ratio was considered to be equal to that in S1.

Table 4
Ash mass balance: percentages of each fraction with respect to the ash fed initially with the fuel (%), mean value and (range of values with λ tested).

	S1	S2/3	Bottom ash	DepC	DepI	Dep	Chim/Ind
PV	23.70 (16.97–29.36)	1.57 (.33–3.09)	**25.27 (18.11–31.32)**	14.74 (8.92–20.87)	6.68 (2.59–11.73)	**21.42 (14.25–27.49)**	53.31 (41.26–66.85)
PVB	22.88 (11.93–50.95)	51.78 (26.71–62.16)	**74.67 (72.78–77.66)**	11.65 (5.82–16.73)	2.03 (1.05–3.07)	**13.68 (6.87–19.60)**	11.65 (6.31–15.47)
PVC	16.97 (8.43–26.82)	33.00 (23.52–40.73)	**49.97 (48.27–50.70)**	5.05 (3.52–7.16)	2.79 (1.26–6.44)	**7.83 (5.73–10.12)**	42.20 (40.72–44.3)
PVCB	22.15 (9.51–33.17)	37.35 (26.21–49.75)	**59.50 (58.42–60.85)**	7.12 (3.98–10.50)	3.56 (2.03–5.14)	**10.68 (6.91–14.11)**	29.82 (26.63–33.72)

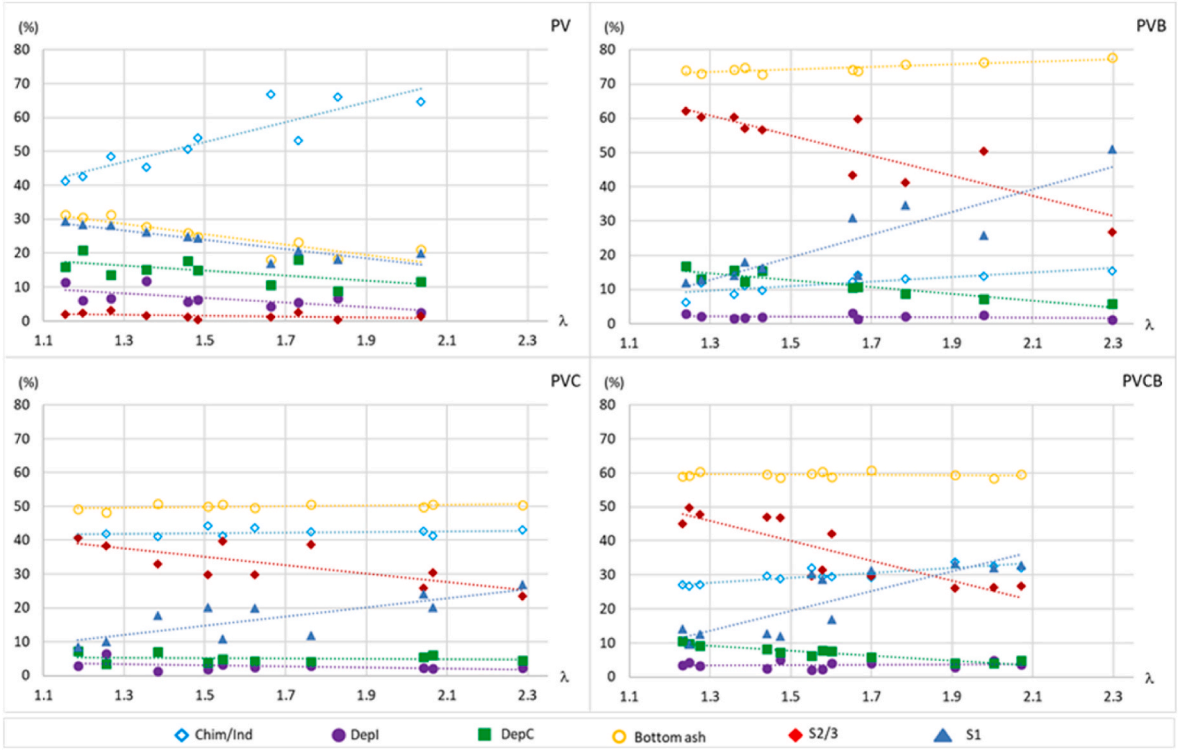

Fig. 3. Ash mass balance (percentages of each of the fractions with respect to the total ash fed with the fuel) for each fuel against λ.

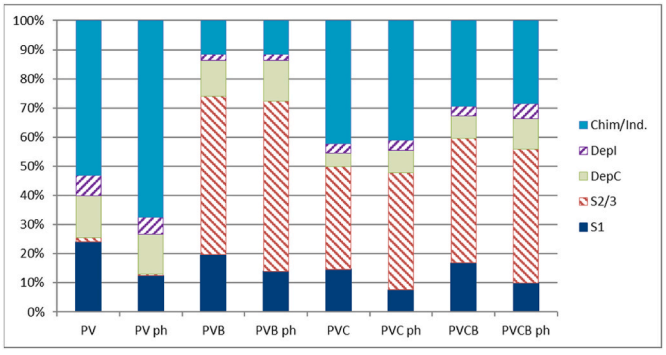

Fig. 4. Ash mass balance for each fuel (percentages of each fraction with respect to the ash fed with the fuel) in tests with air preheating -"ph" tests- (80 °C; average of all the tests) and without air preheating (25 °C; average of the tests with similar λ range to the tests with preheating).

fraction. On the other hand, the amount of each element in DepC is obtained by difference between Dep and DepI values. Note that what DepC fraction actually reflects is the excess of an element in the deposits with respect to the S1 fraction. In K + Na and P, this excess is mostly related to vaporization and subsequent condensation, but in the case of Ca + Mg it may also be related to the greater ease of entrainment, as explained for these two elements in section 1.

Finally, since by definition the composition of the Chim/Ind fraction is unknown, it is set to be the same as the composition obtained in the initial fuel ash analysis (Table 2).

Table 5 presents the mean values of the percentages of each fraction for Si, K + Na, Ca + Mg and P and their range, for each of the four fuels (percentages with respect to the total of the corresponding element; only tests without preheating).

In addition to knowing the range of the percentage of fractions for each element/group of elements, it is also looked closely how they are influenced by λ. The values of each fraction for Si, K + Na, Ca + Mg and P (only tests without preheating) as a function of λ in the cases of PV and PVCB (as a representative fuel of mixed pellets) are shown in Figs. 5 and 6. For supplementary information on the two of them but also on the rest of the mixed pellets, you can refer to Appendix B where the corresponding slope and intercept of the regression lines, as well as the Pearson's coefficient and p-value of the correlations between each fraction and λ are presented.

As done in the case of the ash mass balance, the influence of preheating on the partitioning of each of the elements is analyzed (see Fig. 7).

5. Ash partitioning: analysis

As detected in the previous section, there are important disparities in ash mass balances for the PV and the mixed agropellets, both in ash partitioning (set out in section 4.1) and in elemental partitioning (section 4.2).

It can be seen how in mixed agropellets the bottom-ash-related

Table 5
Elemental mass balance: percentages of the fractions (%) for each element in every fuel, mean value and (range).

		S1	S2/3	Bottom ash	DepC	DepI	Dep	Chim/Ind
Si	**PV**	31.71 (21.03–41.81)	5.69 (1.04–12.82)	**37.40 (24.29–47.85)**	.00 (.00–.00)	8.67 (4.47–14.84)	**8.67 (4.47–14.84)**	53.93 (43.42–67.59)
	PVB	19.34 (9.02–50.48)	68.10 (33.13–82.35)	**87.43 (83.61–92.52)**	.00 (.00–.00)	1.65 (.89–2.66)	**1.65 (0.89–2.66)**	10.92 (5.04–15.34)
	PVC	15.91 (6.02–29.20)	48.00 (37.52–61.83)	**63.91 (56.84–68.85)**	.00 (.00–.00)	2.31 (1.15–4.10)	**2.31 (1.15–4.10)**	33.78 (30.01–40.80)
	PVCB	21.73 (6.82–34.76)	51.57 (38.87–69.75)	**73.29 (67.48–78.60)**	.00 (.00–.00)	3.32 (2.34–4.32)	**3.32 (2.34–4.32)**	23.39 (18.73–28.23)
Ca + Mg	**PV**	27.69 (19.15–38.03)	2.42 (.43–4.62)	**30.11 (20.15–41.72)**	7.15 (4.96–8.47)	7.72 (2.99–13.09)	**14.87 (9.90–21.15)**	55.02 (42.86–69.59)
	PVB	24.51 (13.74–51.39)	59.60 (30.24–73.48)	**84.12 (81.44–88.35)**	.47 (−0.87[a]-1.44)	2.23 (1.06–3.30)	**2.70 (1.22–4.74)**	13.19 (8.04–16.62)
	PVC	18.91 (9.46–30.01)	35.35 (22.60–44.26)	**54.25 (52.48–57.61)**	1.36 (−1.38[a]-3.19)	3.11 (1.46–7.30)	**4.47 (2.75–5.92)**	41.28 (39.29–43.77)
	PVCB	23.58 (10.59–35.19)	40.44 (26.06–56.18)	**64.02 (60.96–67.10)**	2.05 (1.23–3.57)	3.82 (2.09–5.35)	**5.87 (4.67–7.66)**	30.11 (27.12–33.40)
K + Na	**PV**	17.28 (12.64–22.92)	.16 (.04–.32)	**17.44 (12.71–23.04)**	26.39 (12.87–43.29)	5.02 (1.83–10.29)	**31.41 (18.40–45.97)**	51.16 (39.09–66.47)
	PVB	21.12 (9.97–49.06)	28.29 (16.94–34.86)	**49.41 (38.91–66.00)**	40.30 (20.96–53.91)	1.84 (1.02–3.09)	**42.14 (21.98–55.14)**	8.46 (4.01–12.02)
	PVC	11.20 (7.10–16.43)	14.47 (10.22–21.43)	**25.67 (21.41–32.26)**	22.46 (13.91–32.19)	2.06 (.74–5.42)	**24.52 (15.04–34.68)**	49.81 (43.91–57.05)
	PVCB	18.89 (7.14–31.64)	21.83 (15.31–35.38)	**40.73 (32.07–47.65)**	23.76 (11.51–36.86)	3.09 (1.42–5.25)	**26.85 (15.04–39.88)**	32.43 (27.12–39.45)
P	**PV**	27.82 (19.32–37.38)	1.99 (.26–3.60)	**29.81 (19.57–40.84)**	9.49 (7.48–12.39)	7.80 (2.92–13.53)	**17.29 (12.49–22.73)**	52.91 (40.22–67.23)
	PVB	30.12 (14.39–56.14)	47.22 (20.32–68.07)	**77.34 (73.23–82.46)**	2.20 (1.21–4.34)	2.78 (1.16–4.11)	**4.98 (2.95–7.79)**	17.68 (9.75–21.33)
	PVC	15.44 (10.23–21.61)	23.75 (16.16–33.06)	**39.19 (32.74–45.08)**	3.72 (.77–7.79)	2.88 (1.18–7.95)	**6.61 (3.93–9.16)**	54.21 (50.99–60.20)
	PVCB	24.08 (9.92–37.73)	30.98 (16.73–46.50)	**55.06 (50.16–58.19)**	4.79 (3.17–6.78)	3.95 (1.97–6.58)	**8.74 (6.53–11.73)**	36.20 (35.01–38.31)

a. The negative values of Ca + Mg in DepC indicate that the presence of these elements, with respect to Si, is lower in the deposits than in S1.

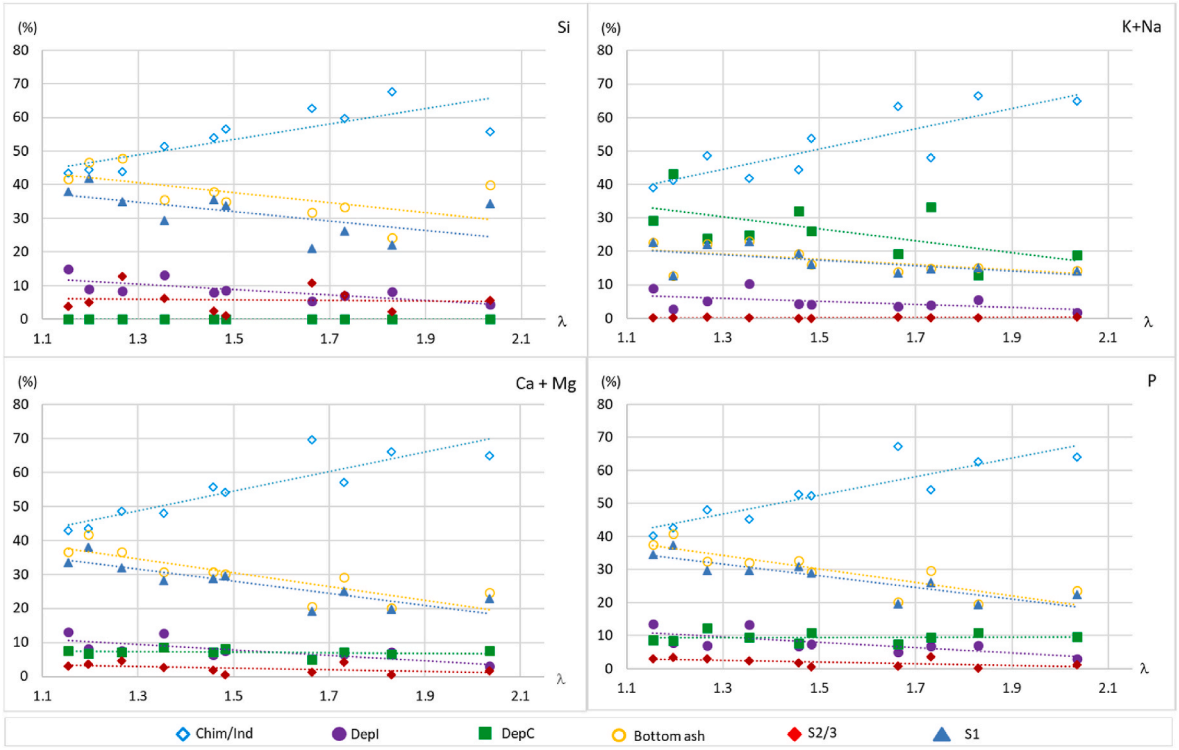

Fig. 5. Elemental mass balance (percentages of the fractions for each element) in PV.

fractions are much higher than the deposition-related fractions (see Table 4): whereas in the former, where the S2/3 fraction generally dominates, and mean percentages between 50 and 75 % are accumulated with both fractions (S1 + S2/3), in the latter, 12 % is not exceeded in the case of DepC and 4 % in that of DepI (Table 4). Regarding the PV, it should be noted that, contrary to what happens in

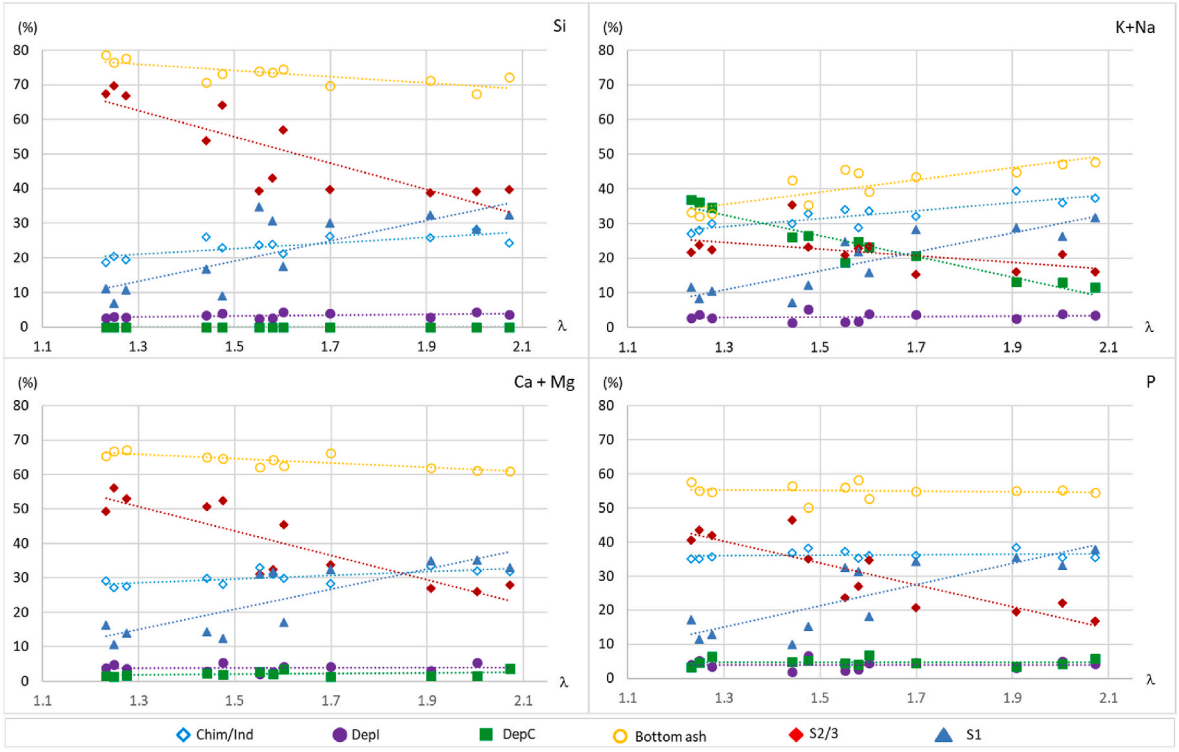

Fig. 6. Elemental mass balance (percentages of the fractions for each element) in PVCB.

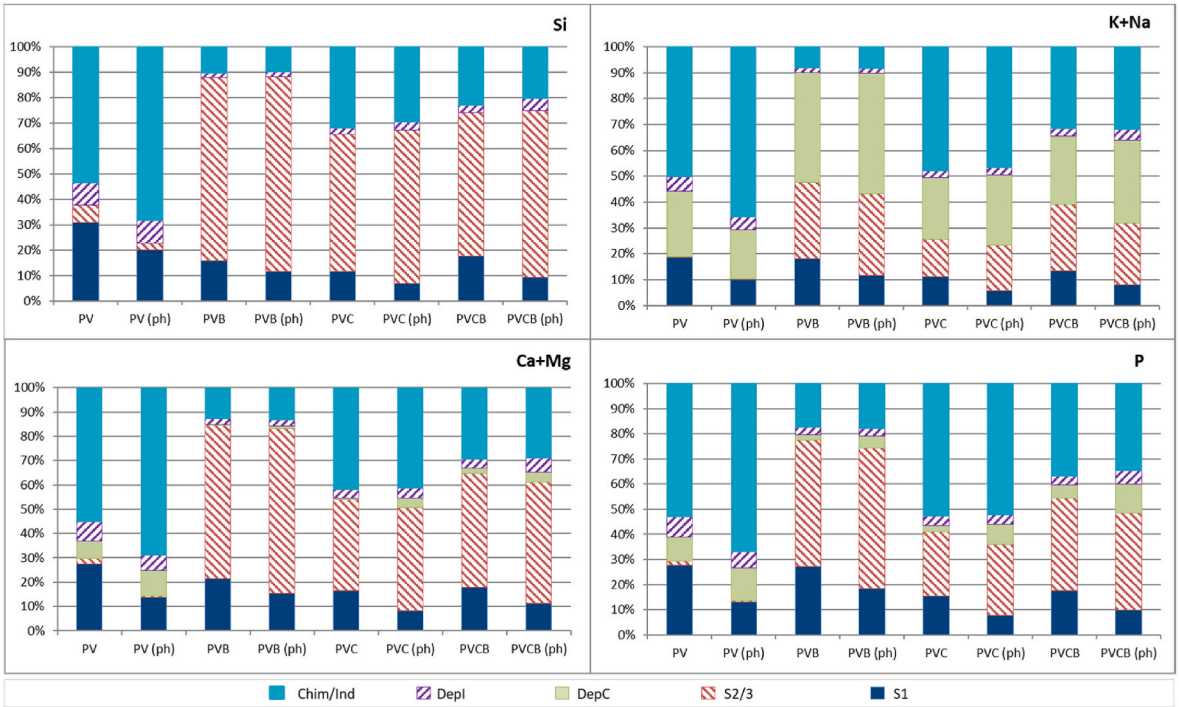

Fig. 7. Elemental mass balance in each fuel (percentages of each fraction with respect to the total element fed with the fuel) in tests with air preheating -"ph" tests- (80 °C; average of all the tests) and without air preheating (25 °C; average of the tests with similar λ range to the tests with preheating).

the case of mixed pellets, the amount of ash that leaves the bed is much greater than that which remains. The dominant fraction is Chim/Ind, as the very low sintering status of the ash leads to the formation of very fine particles [37] that can be easily entrained. For this reason, the DepI fraction is also higher than that of mixed pellets. Possibly due to the substantial K + Na content of this fuel (see Table 2), also the DepC fraction is higher in the PV.

In any case, comparing the results of the four fuels analyzed, it is observed again that the bottom ash fraction is larger as the S2/3 fraction increases, both magnitudes following the same order (PV < PVC < PVCB < PVB), which is due to the aforementioned lesser importance of entrainment in fuels with a greater tendency to sintering.

To delve into all these behaviors, the elemental mass balances are analyzed (see Table 5).

- With regard to Si partitioning, the most refractory element, it can be seen that in the mixed pellets the bottom-ash-related fractions (mainly S2/3) are the major part and always greater than the importance of these fractions in ash mass balance, as this element can only leave the bed by entrainment. Dep fraction is not very relevant, since there is no vaporization/condensation. Chim/Ind fraction of Si is also important in mixed pellets and of the same order of magnitude as in the ash mass balance. In the PV, Chim/Ind fraction is the majority, followed by S1.
- The case of Ca + Mg, also very refractory, is similar to that of Si, but with the Dep fraction being higher and the bottom ash fraction somewhat lower (although still greater than Dep fraction in the ash mass balance). This is due to the already mentioned possible vaporization of Ca + Mg and/or to the fact that part of these elements is released as small micrometer-sized oxides that could be more easily entrained, which is consistent with the fact that for all the agropellets the Chim/Ind fraction is somewhat larger for Ca + Mg than for Si.
- Regarding K + Na, as expected due to the fact that they are the elements with the greatest tendency to vaporize, for the four fuels all the bottom-ash-related fractions show a low value while DepC does the opposite, which causes the Dep fraction to be much higher than that of the rest of the elements and the ash mass balance.
- Due to the fact that P also can form some compounds that vaporize, this element in general presents an intermediate behavior between the most refractory elements (Si and Ca + Mg) and the alkali metals, although closer to the firsts.

5.1. Influence of lambda

With respect to the influence of λ, it should be noted that when λ increases the combustion temperature significantly decreases (TC3m reduces in the order of 200–250 °C for the three mixed agropellets and in the order of 125 °C for PV in tested λ range) and the air velocity in the grate rises (between 12 and 22 % for the mixed agropellets and in the order of 33 % for PV in tested λ range).[5]

As before, two different behaviors can be found when increasing λ (see Fig. 3 and Appendix B): on the one hand, the PV, and on the other, the mixed agropellets. The latter present a very similar trend (same sign of the slopes, although with different values), but the case of PVC stands out as being much less influenced by λ (smaller slope values). This leads to the fact that, for this fuel, in many cases it is not possible to state that the dependence of the different fractions on λ is statistically significant.

In mixed agropellets, while S1 fraction grows substantially in all cases with increasing λ (it more than doubles in PVC, triples in PVCB and quadruples in PVB in the analyzed range), S2/3 fraction decreases by a similar amount (similar slopes but with opposite sign, see Fig. 3 and Appendix B). Thus, bottom ash fraction remains practically constant (only being statistically significant a slight increase in the case of PVB), because the lower combustion temperature involves a lesser vaporization that is compensated by a larger entrainment (the air velocity increases in the grate, along with a reduced sintering). With respect to the fly-ash-related fractions, DepC diminishes with increasing λ, which confirms that due to the decrease in the combustion temperature, less vaporization occurs. On the other hand, the coarse fly ash fraction increases with λ. However, DepI fraction remains practically constant (see Fig. 3 and Appendix B), meanwhile Chim/Ind fraction grows. This may indicate that although there is more entrainment, due to the DepC fraction decrease, in some cases (high λ values) the heat exchange surfaces can start to exhibit symptoms of saturation of inertial impact particles. Given the substantial decrease of the S2/3 fraction together with the increase in air velocity, the ash entrainment could be expected to increment more considerably. To understand this behavior, it must be borne in mind that when λ increases less S2/3 is formed in favour of S1, but in this last fraction can coexist particles of different sizes, from micrometric ones to small agglomerations of particles (as already noted, the only condition is that they pass through a 3.15 mm light sieve), which presents a very different behavior in terms of the possibilities of being entrained.

The case of the PV is quite different from the mixed agropellets, since the amount of bottom ash retained in the bed clearly decreases with increasing λ. This is due to the fact that while the S1 fraction is reduced substantially due to the very high entrainment, the S2/3 fraction remains practically constant (see Fig. 3 and Appendix B) at very low values. The behavior of coarse fly ash fraction is in line with this statement, as clearly increases with λ. The reason for the latter is the aforementioned fineness of a large percentage of the ash particles of this fuel that can be easily entrained. Nevertheless, meanwhile Chim/Ind fraction increases far more than for mixed agropellets (much larger slope value, see Fig. 3 and Appendix B), it should be noted that DepI fraction becomes smaller instead of increasing, and it also does so in parallel to DepC fraction (the trend lines are nearly parallel[6] - see Fig. 3 and Appendix B -). This simultaneous decrease of DepI and DepC seems to strengthen the hypothesis that, although the entrainment is substantially greater, the exchange surfaces can be saturated [36] for all values of λ tested.

In order to delve into all these issues, it is necessary to analyze the partitioning of the main elements that make up the ash depending on the operating conditions.

- The influence of excess air on Si partitioning (Figs. 5 and 6 and Appendix B) is quite similar in each fuel to its influence on ash partitioning (meaning ash mass balance, Fig. 3) except, obviously, in the case of the DepC fraction. It can be highlighted that in all the mixed pellets, as λ increases, so does the S1 fraction of Si while its S2/3 is reduced. In aggregate, the bottom ash fraction of Si decreases with lambda due to higher entrainment, but only slightly. This low influence of increased velocity on entrainment is due to the fact that an important part of the Si has formed alkali metal silicates, with a tendency to form agglomerations, even of relatively small size (passing through a 3.15 mm sieve and therefore classified as S1), which are difficult to entrain.
- The case of Ca + Mg is generally quite similar to that of the Si. In mixed agropellets it is worth noting an even smaller decrease in the bottom ash fraction of Ca + Mg with lambda (a slighter increase in the case of PVC) than in the case of Si (only statistically significant in the case of PVCB, see Appendix B). This behavior is compatible with the already mentioned lower tendency of alkaline earth metals to leave the bed when increasing λ (decreasing the combustion temperature) by vaporization and/or by entrainment.

  Both this fact and the abovementioned tendency of Si to form agglomerates contribute significantly to a lower ash entrainment than could be expected based on the inferior sintering status. This lower-than-expected entrainment comes from the fact that these three elements (Si, Ca and Mg) represent a very high percentage of the total ash in the mixed pellets (see Table 2).
- For K + Na, as happens with the other elements, S1 fraction increases as λ does so in all the mixed pellets, whereas S2/3 fraction decreases. But in this case, taken together, the bottom ash fraction of K + Na

[5] The differences in combustion temperature and air velocity in the grate are calculated from the regression lines of the results obtained in the experimental tests for each fuel.

[6] This result must be taken with certain reservations, since the correlation between DepC and λ presents a p-value somewhat higher than .05.

rises. Most of this increase is explained by the lower vaporization due to the inferior combustion temperature. Thus, for low λ values the DepC fraction of K + Na is the predominant (PVB and PVCB) or only behind the Chim/Ind fraction (PVC), but as λ increases its importance decreases (statistically significant in the case of PVB and PVCB), becoming surpassed by other fractions. In the case of PV, the significant increment in the Chim/Ind fraction of K + Na can be highlighted, mainly due to the large increase in the entrainment phenomenon, since, as already mentioned, the bottom ash of this fuel does not tend to agglomerate.

- With respect to P, the behavior when varying λ is in general similar to that of the most refractory elements (Si and Ca + Mg) for all four fuels. Specifically regarding DepC of P, it should be noted that, unlike what happens with K + Na, it does not show a clear trend in the case of PV, PVB and PVCB but has a statistically relevant positive slope in the case of PVC. To understand this apparently anomalous behavior of PVC, it must be remembered that the DepC fraction reflects the excess in deposition of an element (P in this case) with respect to the composition of S1; therefore, DepC may be influenced by vaporization/condensation (which in this case should decrease), or by entrainment/impact with respect to Si, which in this case seems to present a more pronounced increase than in compounds formed by other elements.

5.2. Influence of inlet air preheating

Regarding inlet air temperature influence, the ash partitioning results in the tests with and without preheating are compared (see Figs. 4 and 7). It should be noted that inlet air preheating has three effects.

- Increases the volumetric flow rate of the air
- Produces an improvement in drying and increases the velocity of the ignition front (around 15–20 % for the different fuels) [35].
- Generates moderated increments in combustion temperatures for mixed agropellets (TC3m variations on the order of +20 °C on average for each fuel) and decreases for PV (TC3m variations in the order of −100 °C on average)

The first two effects produce, for the same value of λ, an increase in air velocity in the grate for the four fuels (around +40 % on average for each mixed pellets and +27 % for PV).

Taking into account also the third effect, unlike the influence of increasing lambda analyzed in section 5.1, for mixed pellets air preheating involves both a growth in air velocity and combustion temperature. This difference will be used to try to delve into the behavior of the ash partitioning for these fuels. In the case of PV, just as when increasing lambda, the air velocity increases and the combustion temperature decreases.

As for mixed pellets, a decrease in bottom ash fraction can be observed in the results of the tests with air preheating shown in Fig. 4. Although there is an increase of S2/3 fraction (+3 to +5 percentage points, that implies only between +7 and +14 %) due to, inter alia, the slight increment in the combustion temperature, it is more than compensated with a clear decrease in S1 fraction (−6 to −7 percentage points, that implies between −30 and −48 %). This fact may be caused by increased entrainment and/or vaporization. When analyzing the fly-ash-related fractions, it is first observed that DepC fraction increases with air preheating for all mixed agropellets, related to the increased vaporization abovementioned. These increments experienced in the S2/3 and DepC fractions could seem higher than expected, given the relatively low variation of the combustion temperature, but they may be again influenced by the improvement in drying and/or the increase of the velocity of the ignition front. DepI fraction slightly grows in PVC and PVCB, and this increment may be related either to the entrainment increase and/or to the fact that, contrary to what happens with increasing λ, as condensation deposition also grows in air preheated tests there are no major saturation problems. Chim/Ind fraction slightly decreases in PVC and PVCB, making overall the coarse fly ash fraction does not present a clear trend. In order to finally determine if there is an increase in ash entrainment, the analysis of the elemental partitioning, which will be carried out below, becomes very helpful.

From the mass balances of all the elements considered here, it can be verified (Fig. 7) that also an increase in the S2/3 fraction (except for K + Na in PVCB) and an important decrease in S1 are observed in all the mixed pellets. Similarly, an increment in the DepC fraction is also observed for K + Na, Ca + Mg and P, due to the greater vaporization (and/or entrainment in the case of Ca + Mg). Among these increments, it is worth highlighting the very pronounced growth of P, which is compatible with an increase in vaporization added to a greater ease of entrainment, as is commented for λ variation at the end of section 5.1. Closely related to the DepC increase, as was the case when analyzing the ash partitioning, it can be seen that the DepI fraction grows in all the mixed pellets and for all the elements (except for K + Na in PVB and P in PVB and PVC, which remain practically constant), which confirms that in these conditions there are no saturation phenomena.

However, the most interesting point to analyze in the elemental mass balances in mixed pellets is the behavior of the bottom ash fraction. In its focus on Si, which can only leave the bed by entrainment, the bottom ash fraction increases, as a consequence of two opposing effects: the higher air velocity more than compensated for the increased entrainment difficulty due to the higher sintering status. In the case of K + Na, preheating produces a decrease in the bottom ash fraction, which is due, in addition to the two opposite effects mentioned for Si, to the fact that the increase in combustion temperature as well as the improvement in drying and the increment of the velocity of the ignition front, produces greater vaporization of compounds containing these elements. Regarding Ca + Mg there is also a decrease in the bottom ash fraction, which confirms the aforementioned possible slight vaporization of these elements and/or a greater formation of micrometric particles, linked in both cases to the rise in combustion temperature. All of this suggests that, due to the increase in sintering status, the increment in air velocity that preheating implies does not cause a higher entrainment, except perhaps in the case of some particles containing Ca + Mg and P. This result could not have been obtained without the analysis of the elemental partitioning.

Regarding the effect of preheating in the case of PV, given that both the variation in combustion temperature and air velocity are comparable to those that occurred when increasing λ, the analysis of ash and elemental mass balances are similar to that already done in section 5.1. The coherence of this result supports the use of the tests with air preheating to better understand and confirm the partitioning trends of the mixed pellets.

6. Conclusions

In this paper, the development of an extended methodology applicable to any biomass fuel to analyze the ash partitioning is presented. To its application, it is required to collect certain specific samples from tests in a combustion equipment and analyze them through SEM-EDS technique, which allows splitting the fuel ash into five fractions (S1, S2/3, Depc, DepI and Chim/Ind), by using a complete ash mass balance but also an elemental distribution. The inclusion in this methodology of two fractions related to deposition (DepC and DepI), based on the mechanisms by which the ash can leave the bed (vaporization and entrainment), represents a step forward and helps to better understand the ash partitioning.

This methodology has been applied as an example to four agropellets made of three agricultural residual biomasses: one woody pellet and three others composed by blend with a herbaceous component (mixed agropellets). As a result, both the values of each of the mentioned fractions and the influence of the operation conditions on them have been obtained. Based on the average results of the elemental mass

balance, it can be stated that the retention in the bed (S1 + S2/3) of each studied element follows the same order in all the analyzed fuels: Si > Ca + Mg > P > K + Na. On the contrary, the exact inverse order is observed in the deposition ash fraction value (Dep) of each element.

As the main idea, combining the results of both types of mass balances with the variations in λ and inlet air temperature, it has been corroborated that incrementing the excess air in tested range, which means an increase in the air velocity in the grate and a decrease in the combustion temperature, improve the behavior of the mixed agropellets both in sintering (decrease in S2/3 fraction) and in deposition (decrease in DepC and not increase in DepI fractions). The reduction in boiler performance which arises from using high excess air ratios can be minimized with the use of condensing boilers.

In case of the woody pellet, as its much lower sintering status involves a dominance of fractions related with entrainment (Chim/Ind and DepI), it is preferable, contrary to the case of mixed pellets, working with low excess air.

As can be concluded, for the correct use of each fuel it is necessary to consider the varying amount of each of the ash fractions as well as their composition, since they affect both the optimal boiler operation (mainly the excess air used), as well as the proper sizing and design of several of its systems (grate, bottom ash removal, ashtray, tube cleaning, particle capture, etc.). Therefore, it is hoped that the methodology for the study of the ash partitioning presented here can contribute to understand ash and elemental behavior and to find strategies to achieve greater use of varied agricultural residual biomass in the domestic sector. Additionally, this methodology, which does not require very complex analysis techniques (sampling, weighing and SEM-EDS analysis), can also serve as a starting point for the subsequent development of a more standard methodology to determine the biomass ash partitioning in a specific facility, which allows obtaining its optimal operating conditions.

Complementarily, this acquired knowledge relative to elemental partitioning could increase the chances of finding new subsequent applications for the suitable ash fractions. Some possibilities may be their use as soil conditioner, fertilizer additive or construction material, where woody and/or agricultural residual biomass ash could fit, but much more research is still required [54].

CRediT authorship contribution statement

Javier Royo: Writing – review & editing, Writing – original draft, Validation, Supervision, Project administration, Methodology, Investigation, Funding acquisition, Formal analysis, Data curation, Conceptualization. **Paula Canalís:** Writing – review & editing, Writing – original draft, Validation, Methodology, Investigation, Formal analysis, Data curation, Conceptualization. **David Quintana:** Writing – review & editing, Writing – original draft, Validation, Methodology, Investigation, Formal analysis, Data curation, Conceptualization.

Acknowledgements

The authors greatly acknowledge the Spanish Ministry of Science and Innovation and the Spanish Ministry of Universities for funding the project "MHWPellet: Mixed pellets based on agricultural crops residues (herbaceous and woody) for their use in the residential sector: optimization of their composition and conversion parameters" (ref. ENE2015-68809-R (MIMECO/FEDER, UE)).

Authors also would like to acknowledge the use of *Servicio General de Apoyo a la Investigación-SAI, Universidad de Zaragoza.*

APPENDIX A

This appendix presents a sensitivity analysis of the value of the heat exchange surface per unit of heat transfer ratio (specific area, varying between .06 and .12 $m^2\ kW^{-1}$) on ash partitioning.

Fig. A1 shows the PVCB's ash partitioning for different values of the specific area. It can be observed that the relationship between DepC and DepI remains constant in all cases.

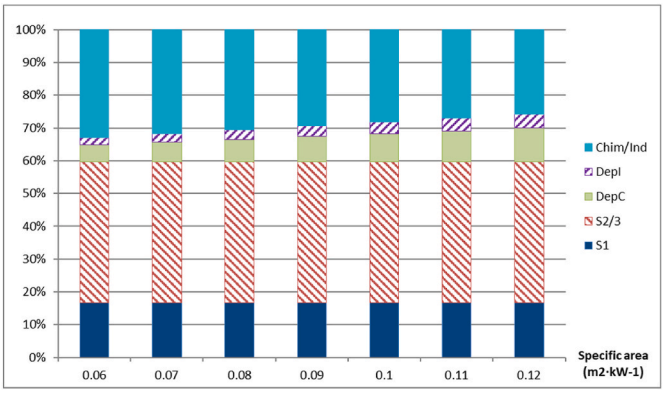

Fig. A1. PVCB's ash partitioning for different values of the specific area (m^2·kW^{-1}).

Fig. A2 shows the DepC fraction percentage for PVCB as a function of λ. As the specific area increases, the trends are maintained, with only greater slopes of the regression lines.

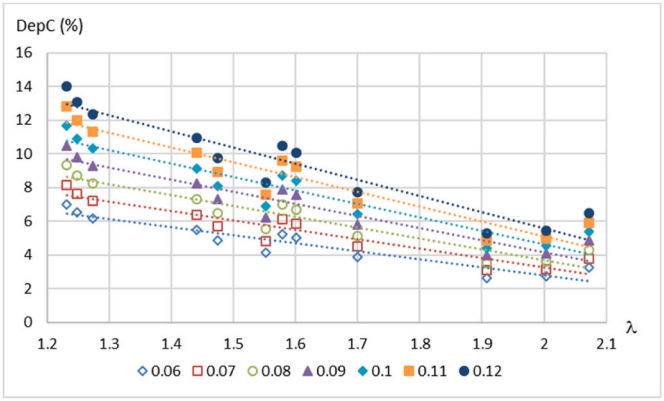

Fig. A2. DepC fraction (%) for the PVCB for different values of the specific area ($m^2 \cdot kW^{-1}$) as a function of λ.

Fig. A3 shows the mean percentage of the DepC fraction with different specific area values for the four fuels analyzed. It can be verified how the proportions between the different fuels are maintained.

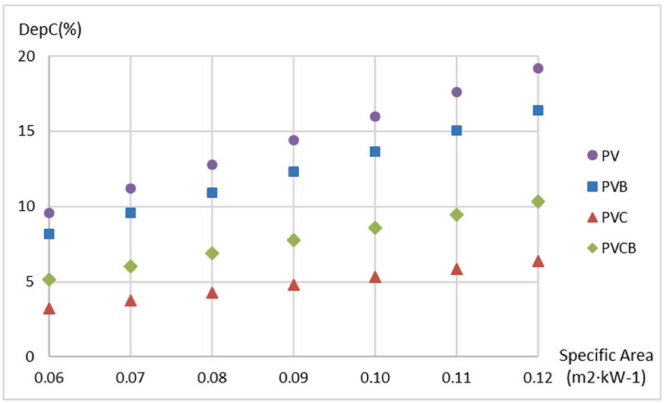

Fig. A3. Mean DepC fraction (%) with different specific area values for the four fuels analyzed ($m^2 \cdot kW^{-1}$).

APPENDIX B

Table B1 presents, for all agropellets, the corresponding slope and intercept of the regression lines, as well as the Pearson's coefficient and p-value of the correlations between λ and each fraction of the ash partitioning (corresponds to Fig. 3) and elemental partitioning (PV and PVCB data corresponds to Figs. 5 and 6).

With this data it is possible to determine whether the correlations are considered statistically significant and their relevance. Regarding the intercept, the parameter Inter 1.5 is presented here, which is the value (%) of the corresponding fraction obtained from the trend line for a λ of 1.5; together with the slope, it is possible to reproduce the trend line and estimate the value of each fraction for any value of λ in tested range.

Table B1
Ash and elemental partitioning: slope and intercept (for a λ value of 1.5) of the regression lines, Pearson's Coefficient (r) and P-values (p) of the correlations between each fraction and λ.

	S1				S2/3				Bottom Ash				DepC				DepI				Chim/Ind			
	r	p	Slope	Int 1.5	r	p	Slope	Int 1.5	r	p	Slope	Int 1.5	r	p	Slope	Int 1.5	r	p	Slope	Int 1.5	r	p	Slope	Int 1.5
Ash																								
PV	.89	<.001	−13.8	23.9	.46	.184	−1.4	1.6	.88	<.001	−15.2	25.5	.59	.072	−7.5	14.9	.67	.036	−6.6	6.8	.89	<.001	29.2	52.8
PVB	.88	<.001	33.1	19.3	.87	.001	−29.3	54.9	.85	.002	3.8	74.3	.93	<.001	−10.0	12.7	.26	.460	−.5	2.1	.82	.004	6.7	10.9
PVC	.78	.007	13.5	14.7	.75	.013	−12.4	35.1	.50	.140	1.1	49.8	.16	.664	−.6	5.1	.40	.255	−1.5	3.0	.31	.377	1.0	42.0
PVCB	.84	<.001	29.1	19.5	.87	<.001	−29.4	40.0	.13	.681	−.3	59.5	.94	<.001	−7.2	7.8	.12	.699	.4	3.5	.87	<.001	7.1	29.2
Si																								
PV	.60	.069	−14.0	32.0	.07	.848	−.9	5.7	.61	.059	−14.9	37.7	0	N/A	0	0	.73	.016	−8.0	8.8	.80	.005	22.9	53.5
PVB	.82	.004	31.5	15.9	.86	.002	−38.7	72.2	.77	.009	−7.1	88.2	0	N/A	0	0	.25	.478	−.4	1.7	.77	.009	7.6	10.1
PVC	.81	.005	18.8	12.8	.79	.006	−21.0	51.5	.19	.597	−2.2	64.3	0	N/A	0	0	.03	.942	−.1	2.3	.20	.575	2.3	33.4
PVCB	.78	.003	29.0	19.1	.84	<.001	−37.9	55.0	.77	.003	−8.9	74.1	0	N/A	0	0	.42	.175	1.0	3.2	.76	.004	7.9	22.7
Ca + Mg																								
PV	.85	.002	−17.7	28.0	.50	.141	−2.5	2.5	.84	.002	−20.2	30.5	.23	.514	−.8	7.2	.74	.015	−7.9	7.9	.89	<.001	28.9	54.5
PVB	.90	<.001	33.2	21.0	.90	<.001	−37.8	63.7	.61	.061	−4.7	84.6	.41	.237	−.8	.6	.31	.384	−.7	2.3	.76	.011	6.2	12.5
PVC	.77	.010	14.8	16.5	.73	.017	−14.6	37.8	.05	.891	.2	54.2	.65	.041	2.2	1.0	.41	.243	−1.8	3.4	.20	.582	−.7	41.4
PVCB	.83	<.001	29.2	20.9	.87	<.001	−35.5	43.7	.82	.001	−6.3	64.6	.32	.318	.9	2.0	.03	.915	.1	3.8	.70	.010	5.3	29.6
K + Na																								
PV	.58	.079	−8.1	17.4	.48	.157	.2	.2	.57	.086	−7.9	17.6	.60	.065	−17.9	26.7	.50	.146	−4.5	5.1	.85	.002	30.2	50.6
PVB	.86	.001	32.5	17.6	.53	.118	−8.7	29.2	.89	<.001	23.7	46.9	.92	<.001	−29.5	43.5	.17	.643	−.3	1.9	.81	.004	6.1	7.8
PVC	.60	.068	4.6	10.4	.03	.938	−.2	14.5	.42	.223	4.4	24.9	.52	.123	−9.5	24.0	.50	.137	−1.9	2.4	.57	.088	7.0	48.7
PVCB	.87	<.001	27.3	16.4	.52	.082	−9.6	22.7	.86	<.001	17.7	39.1	.96	<.001	−29.9	26.5	.16	.629	.6	3.0	.87	<.001	11.6	31.4
P																								
PV	.86	.002	−17.8	28.1	.58	.080	−2.5	2.0	.85	.002	−20.3	30.2	.02	.956	.1	9.5	.71	.022	−8.0	7.9	.89	<.001	28.2	52.4
PVB	.81	.005	31.5	26.7	.79	.006	−34.1	50.9	.31	.383	−2.6	77.6	.49	.153	−1.3	2.3	.51	.134	−1.3	2.9	.51	.135	5.2	17.1
PVC	.39	.270	3.9	14.8	.57	.087	−8.1	25.1	.42	.226	−4.2	39.9	.77	.009	4.8	2.9	.54	.109	−3.0	3.4	.31	.378	2.4	53.8
PVCB	.83	<.001	31.2	21.3	.87	<.001	−32.1	33.9	.12	.717	−.9	55.1	0	.989	0	4.8	.03	.926	.1	3.9	.18	.567	.7	36.1

Data availability

Data will be made available on request.

References

[1] European Commission, A policy framework for climate and energy in the period from 2020 to 2030 (COM (2014) 15 final). Communication from the Commission to the European Parliament, the Council, the European Economic and Social Committee and the Committee of the Regions, 2014.

[2] N. Scarlat, F. Fahl, E. Lugato, F. Monforti-Ferrario, J.F. Dallemand, Integrated and spatially explicit assessment of sustainable crop residues potential in Europe, Biomass Bioenergy 122 (2019) 257–269.

[3] Ch Weiser, V. Zeller, F. Reinicke, B. Wagner, S. Majer, A. Vetter, D. Thraen, Integrated assessment of sustainable cereal straw potential and different straw-based energy applications in Germany, Appl. Energy 114 (2014) 749–762.

[4] N. Scarlat, M. Martinov, J.F. Dallemand, Assessment of the availability of agricultural crop residues in the European Union: potential and limitations for bioenergy use, Waste Management 30 (2010) 1889–1897.

[5] L. Carvalho, E. Wopienka, C. Pointner, J. Lundgren, V.K. Verma, W. Haslinger, C. Schamidl, Performance of a pellet boiler fired with agricultural fuels, Appl. Energy 104 (2013) 286–296.

[6] L. Wang, G. Skjevrak, J.E. Hustad, M. Gronli, O. Skreiberg, Effects of additives on barley straw and husk ashes sintering characteristics, Energy Proc. 20 (2012) 30–39.

[7] O. Sippula, K. Hytönen, J. Tissari, T. Raunemaa, J. Jokiniemi, Effect of wood fuel on the emissions from a top-feed pellet stove, Energy & Fuels 21 (2) (2007) 1151–1160.

[8] E. Houshfar, T. Lovas, O. Skreiberg, Experimental investigation on NOX reduction by primary measures in biomass combustion: straw, peat, sewage sludge, forest residues and wood pellets, Energies 5 (2) (2012) 270–290.

[9] M. Díaz-Ramírez, F. Sebastian, J. Royo, A. Rezeau, Influencing factors on NOX emission level during grate conversion of three pelletized energy crops, Appl. Energy 115 (0) (2014) 360–373.

[10] D. Boström, N. Skoglund, A. Grimm, C. Boman, M. Ohman, M. Brostrom, R. Backman, Ash transformation chemistry during combustion of biomass, Energy & Fuels 26 (2012) 85–93.

[11] S.V. Vassilev, B. Baxter, L.K. Andersen, C.G. Vassileva, An overview of the chemical composition of biomass, Fuel 89 (2010) 913–933.

[12] S.V. Vassilev, C.G. Vassileva, Methods for characterization of composition of fly ashes from coal-fired power stations: a critical overview, Energy & Fuels 19 (2005) 1084–1098.

[13] D. Boström, A. Grimm, C. Boman, E. Björnbom, M. Öhman, Influence of kaolin and calcite additives on ash transformations in small-scale combustion of oat, Energy Fuels 23 (10) (2009) 5184–5190.

[14] M. Díaz-Ramírez, C. Boman, F. Sebastian, J. Royo, S. Xiong, D. Boström, Ash characterization and transformation behavior of the fixed-bed combustion of novel crops: poplar, Brassica, and cassava fuels, Energy & Fuels 26 (6) (2012) 3218–3229.

[15] M. Díaz-Ramírez, F.J. Frandsen, P. Glarborg, F. Sebastian, J. Royo, Partitioning of K, Cl, S and P during combustion of poplar and brassica energy crops, Fuel 134 (0) (2014) 209–219.

[16] U. Kleinhans, Ch Wieland, F.J. Frandsen, H. Spliethoff, Ash formation and deposition in coal and biomass fired combustion systems: progress and challenges in the field of ash particle sticking and rebound behaviour, Prog. Energy Combust. Sci. 68 (2018) 65–168.

[17] N. Sonoyama, T. Okuno, O. Masek, S. Hosokai, Ch Li, J. Hayashi, Interparticle desorption and Re-adsorption of alkali and alkaline earth metallic species within a bed of pyrolyzing char from pulverized woody biomass, Energy & Fuels 20 (2006) 1294–1297.

[18] M.K. Misra, K.W. Ragland, A.J. Baker, Wood ash composition as a function of furnace temperature, Biomass Bioenergy 4 (2) (1993) 103–116, https://doi.org/10.1016/0961-9534(93)90032-Y.

[19] M. Bilton, A.P. Brown, S.J. Milne, Investigating the optimum conditions for the formation of calcium oxide, used for CO2 sequestration, by thermal decomposition of calcium acetate, J. Phys. Conf. 371 (2012), https://doi.org/10.1088/1742-6596/371/1/012075.

[20] S.V. Vassilev, B. Baxter, C.G. Vassileva, An overview of the behaviour of biomass during combustion: Part I. Phase-mineral transformations of organic and inorganic matter, Fuel 112 (2013) 391–449.

[21] P. Glarbor, P. Marshall, Mechanism and modeling of the formation of gaseous alkali sulfates, Combust. Flame 141 (2005) 22–39.

[22] M.U. Garba, D.B. Ingham, L. Ma, R.T.J. Porter, M. Pourkashnian, H.Z. Tan, A. Williams, Prediction of Potassium Chloride Sulfation and its Effect on Deposition in Biomass-Fired Boilers EnergyFuels, vol. 26, 2012, pp. 6501–6508.

[23] Y. Niu, H. Tan, S. Hui, Ash-related issues during biomass: alkali-induced slagging, silicate melt-induced slagging (ash fusion), agglomeration, corrosion, ash utilization, and related countermeasures, Prog. Energy Combust. Sci. 52 (2016) 1–61.

[24] J. Capablo, Formation of alkali salt deposits in biomass combustion, Fuel Process. Technol. 153 (2016) 58–73.

[25] A. Junemann, G. Legarreta, Inhalación de humo de leña: una causa relevante pero poco reconocida de Enfermedad Pulmonar Obstructiva Crónica, Revista Argentina de Medicina Respiratoria 2 (2007 - Nº) 51–57.

[26] D. Tian, Y. Hu, Y. Wang, J.W. Boylan, M. Zheng, A.G. Russell, Assessment of biomass burning emissions and their impacts on urban and regional PM2.5: a Georgia case study, Environmental Science Technology 43 (2009) 299–305.

[27] X. Yang, D. Lu, B. Zhu, Z. Sun, G. Li, J. Li, Q. Liu, G. Jiang, Phase transformation of silica particles in coal and biomass combustion processes, Environmental Pollution 292 (2022) 118312.

[28] K.A. Christensen, M. Stenholm, H. Livbjerg, The formation of submicron aerosol particles, HCl and SO2 in straw-fired boilers, Aerosol Science 29 (4) (1998) 421–444.

[29] T. Saud, T.K. Mandal, R. Gadi, D.P. Singh, S.K. Sharma, M. Saxena, A. Mukherjee, Emission estimates of particulate matter (PM) and trace gases (SO2, NO and NO2) from biomass fuels used in rural sector of Indo-Gangetic Plain, India, Atmos. Environ. 45 (32) (2011) 5913–5923.

[30] J. Falk, T.K. Hannl, M. Öhman, A. Hedayati, N. Skoglund, Ash transformation during fixed-bed Co-combustion of sewage sludge and agricultural residues with a focus on phosphorus, ACS Omega 8 (2023) 13162–13176.

[31] P. Teixeira, H. Lopes, I. Gulyurtlu, N. Lapa, Use of chemical fractionation to understand partitioning of biomass ash constituents during co-firing in fluidized bed combustion, Fuel 101 (2012) 215–227.

[32] A. Hedayati, J. Falk, E. Borén, R. Lindgren, N. Skoglund, Ch Boman, M. Öhman, Ash transformation during fixed-bed combustion of agricultural biomass with a focus on potassium and phosphorus, Energy Fuels 36 (2022) 3640–3653.

[33] A.J. Damoe, P.A. Jensen, F.J. Frandsen, H. Wu, P. Glarborg, Fly ash formation during suspension firing of biomass: effects of residence time and fuel type, Energy Fuels 31 (2017) 555–570.

[34] S. Pachchigar, T.K. Hannl, M. Öhman, Ash Formation during combustion of rice husks in entrained flow conversion conditions, Energy Fuels 38 (2024) 13278–13294.

[35] J. Royo, P. Canalís, D. Quintana, M. Díaz-Ramírez, A. Sin, A. Rezeau, Experimental study on the ash behaviour in combustion of pelletized residual agricultural biomass, Fuel 239 (2019) 991–1000.

[36] J. Royo, P. Canalís, D. Quintana, Chemical study of fly ash deposition in combustion of pelletized residual agricultural biomass, Fuel 268 (2020) 117–228.

[37] J. Royo, P. Canalís, D. Quintana, Chemical study of bottom ash sintering in combustion of pelletized residual agricultural biomass, Fuel 310 (Part B) (2022) 122145.

[38] M. Díaz-Ramirez, D. Maraver, A. Rezeau, J. Royo, S. Sala, F. Sebastian, A. Sin, Estimation of the deposition on trigeneration system components fueled by ash rich biomass. Proceedings of 20th European Biomass Conference and Exhibition, Milan, Italy, 2012, pp. 774–780.

[39] L.J.R. Nunes, J.C.O. Matias, J.P.S. Catalao, Biomass combustion systems: a review on the physical and chemical properties of the ashes, Renew. Sustain. Energy Rev. 53 (2016) 235–242.

[40] T. Zeng, T. Pollex, N. Weller, V. Lenz, M. Nelles, Blended biomass pellets as fuel for small scale combustion appliances: effect of blending on slag formation in the bottom ash and pre-evaluation options, Fuel 212 (2018) 108–116.

[41] M. Öhmana, C. Bomana, H. Hedmanb, A. Nordina, D. Boström, Slagging tendencies of wood pellet ash during combustion in residential pellet burners, Biomass Bioenergy 27 (2004) 585–596.

[42] E. Lindström, M. Sandström, D. Boström, M. Öhman, Slagging characteristics during combustion of cereal grains rich in phosphorus, Energy & Fuels 21 (2007) 710–717.

[43] M. Theis, B.J. Skrifvars, M. Hupa, H. Tran, Fouling tendency of ash resulting from burning mixtures of biofuels. Part 1: deposition rates, Fuel 85 (2006) 1125–1130.

[44] P.A. Jensen, M. Stenholm, P. Hald, Deposition investigation in straw-fired boilers, Energy Fuels 11 (1997) 1048–1055.

[45] H. Kaufmann, T. Nussbaumer, L. Baxter, N. Yang, Deposit formation on a single cylinder during combustion of herbaceous biomass, Fuel 79 (2000) 141–151.

[46] R. Weber, Y. Poyraz, M. Beckmann, S. Brinker, Combustion of Biomass in Jet Flames, vol. 35, Proceedings of the Combustion Institute, 2015, pp. 2749–2758.

[47] S.S. Lokare, J.D. Dunaway, D. Moulton, D. Rogers, D.R. Tree, L.L. Baxter, Investigation of ash deposition rates for a suite of biomass fuels and fuel blends, Energy Fuel. 20 (3) (2006) 1008–1014.

[48] A. Regueiro, D. Patiño, E. Granda, J. Porteiro, Experimental study on the fouling behaviour of an underfeed fixed-bed biomass combustor, Appl. Therm. Eng. 112 (2017) 523–533.

[49] L. Wang, O. Skreiberg, M. Becidan, Investigation of additives for preventing ash fouling and sintering during barley straw combustion, Appl. Therm. Eng. 70 (2014) 1262–1269.

[50] L. Deng, X. Jin, J. Long, D. Che, Ash deposition behaviors during combustion of raw and water washed biomass fuels, J. Energy Inst. 92–4 (2019) 959–970.

[51] H.B. Dizaji, T. Zeng, H. Hölzig, J. Bauer, G. Klös, D. Enke, Ash transformation mechanism during combustion of rice husk and rice straw, Fuel 307 (2022) 121768.

[52] M. Zevenhoven, P. Yrjas, B.J. Skrifvars, M. Hupa, Characterization of ash-forming matter in various solid fuels by selective leaching and its implications for fluidized-bed combustion, Energy Fuel. 26 (2012) 6366–6386.

[53] Dimian AC, Bildea CS. Chemical process design: computer-aided case studies. First published: 20 February 2008. Print - ISBN:9783527314034, Online - ISBN: 9783527621583, DOI:10.1002/9783527621583, Copyright © 2008 Wiley-VCH Verlag GmbH & Co. KGaA.

[54] J. Zhai, I.T. Burke, D.I. Stewart, Beneficial management of biomass combustion ashes, Renew. Sustain. Energy Rev. 151 (2021) 111555.